Water Science and Engineering 2022, 15(3): 179−188

HOSTED BY

ELSEVIER

Available online at www.sciencedirect.com

Water Science and Engineering

journal homepage: wse.hhu.edu.cn

Evaluating performance dependency of a geomorphologic instantaneous unit hydrograph-based hydrological model on DEM resolution

Cheng Yao [a], Zhi-jia Li [a], Ke Zhang [a,b,c,d,*], Ying-chun Huang [a], Jing-feng Wang [a,e], Satish Bastola [f]

[a] College of Hydrology and Water Resources, Hohai University, Nanjing 210098, China
[b] Yangtze Institute for Conservation and Development, Hohai University, Nanjing 210098, China
[c] State Key Laboratory of Hydrology−Water Resources and Hydraulic Engineering, Hohai University, Nanjing 210098, China
[d] China Meteorological Administration−Hohai University Joint Laboratory for Hydrometeorological Studies, Hohai University, Nanjing 210098, China
[e] School of Civil and Environmental Engineering, Georgia Institute of Technology, Atlanta 30332, USA
[f] Department of Civil and Environmental Engineering, University of New Orleans, New Orleans 70148, USA

Received 20 October 2021; accepted 24 March 2022
Available online 30 April 2022

Abstract

The digital elevation model (DEM) is a type of model that has been widely used in terrain analysis and hydrological modeling. DEM resolution influences the hydrological and geomorphologic features of delineated catchments and consequently affects hydrological simulations. This study investigated the impacts of DEM resolution on the performance of the XAJ-GIUH hydrological model, a model coupling the widely used Xinanjiang (XAJ) hydrological model with the geomorphologic instantaneous unit hydrograph (GIUH), in flood simulations in small and medium-sized catchments. To test the model performance, the model parameters were calibrated at a fine DEM resolution (30 m) and then directly transferred to the simulation runs using coarser DEMs. Afterwards, model recalibration was conducted at coarser DEM resolutions. In the simulation runs with the model parameters calibrated at the 30-m resolution, the DEM resolution slightly affected the overall shape of the simulated flood hydrographs but presented a greater impact on the simulated peak discharges in the two study catchments. The XAJ-GIUH model consistently underestimated the peak discharges when the DEM resolution became coarser. The qualified ratio of peak simulations decreased by 35% when the DEM resolution changed from 30 m to 600 m. However, model recalibration produced comparable model performances when DEMs with different resolutions were used. This study showed that the impact of DEM resolution on model performance can be mitigated by model recalibration to some extent, if the DEM resolution is not too coarse.
© 2022 Hohai University. Production and hosting by Elsevier B.V. This is an open access article under the CC BY-NC-ND license (http://creativecommons.org/licenses/by-nc-nd/4.0/).

Keywords: DEM resolution; XAJ-GIUH model; Flood simulation; Model recalibration; Small and medium-sized catchments

1. Introduction

The digital elevation model (DEM), a digital representation of continuous topography, constitutes key input data for representations of the topographic characteristics of a catchment (Vieux, 2001; Zheng et al., 2018). With the increasing availability of the DEM data, DEMs have been extensively used in hydrological studies, including the development of hydrological models, examinations of hydrological processes, and construction of operational hydrological forecasting systems (Zhang et al., 2016; Blair et al., 2019; Khaing et al., 2019; Yao et al., 2019; Chao et al., 2021; Mu et al., 2021; Xu, 2021). This has raised the question of the effect of DEM resolution on the performance of hydrological models. Hydrologists have been widely interested in analyzing the sensitivity of DEM-based models to the DEM resolution

This work was supported by the National Natural Science Foundation of China (Grants No. 51979070 and 52079035), the National Key Research and Development Program of China (Grant No. 2018YFC1508103), the Natural Science Foundation of Jiangsu Province (Grant No. BK20180022), and the Six Talent Peaks Project in Jiangsu Province (Grant No. NY-004).
* Corresponding author.
E-mail address: kzhang@hhu.edu.cn (Ke Zhang).
Peer review under responsibility of Hohai University.

https://doi.org/10.1016/j.wse.2022.04.002
1674-2370/© 2022 Hohai University. Production and hosting by Elsevier B.V. This is an open access article under the CC BY-NC-ND license (http://creativecommons.org/licenses/by-nc-nd/4.0/).

(Valeo and Moin, 2000; Dixon and Earls, 2009; Beven, 2012; Clark et al., 2017; Wilby, 2019; Zha et al., 2021).

To assess the effect of DEM resolution, Chaubey et al. (2005) ran the SWAT model at seven resolutions ranging from 30 m to 1 000 m and found that a greater grid size (i.e., coarser resolution) resulted in decreased streamflow, probably due to the reduced total watershed area, flattened watershed slope, and increased slope length. Reddy and Reddy (2015) also investigated the DEM resolution's impact on the performance of the SWAT model and concluded that varying DEM resolutions resulted in considerable variability in simulated daily runoff and sediment yields. Yang et al. (2014) assessed the effects of five LiDAR-derived DEM data sets with different resolutions on the extraction of hydrographic features and the performance of the hydrological simulation program−Fortran (HSPF) model. They demonstrated that more accurate representations of the stream network and watershed boundary can be obtained from DEMs with finer resolutions. However, the HSPF model did not necessarily produce better daily simulations using DEMs with higher resolutions. Habtezion et al. (2016) applied an overland flow model to a large Prairie Pothole region using four DEM data sets with different resolutions to examine the impacts of DEM resolution. They found that simulations with coarser DEMs tended to overestimate the ponded areas and underestimate the peak discharges. Many similar studies have been carried out in recent years. These studies suggest that assessment of the DEM resolution's impact is necessary to achieve better implementation of DEM-based hydrological models (Moglen and Hartman, 2001; Vivoni et al., 2005; López-Vicente and Álvarez, 2018; Beven, 2019; Chao et al., 2019; Munoth and Goyal, 2019; Zhu et al., 2020; Wei et al., 2021; Zhang et al., 2021).

To consider the effect of geomorphologic characteristics on runoff routing, Rodriguez-Iturbe and Valdes (1979) and Gupta et al. (1980) proposed the geomorphologic instantaneous unit hydrograph (GIUH) routing approach. It has been demonstrated that the GIUH approach has the advantage of linking hydrologic responses to the geomorphologic characteristics of catchments (DaRos and Borga, 1997). Thus, the GIUH approach, which can be easily derived from DEM, is efficient and effective when applied to ungauged basins (Bhadra et al., 2008; Grimaldi et al., 2012; Hrachowitz et al., 2013). To improve the flood prediction capability of the well-known Xinanjiang (XAJ) model (Zhao, 1992; Zhao and Liu, 1995; Yao et al., 2009, 2012; Gong et al., 2021) for ungauged catchments, Yao et al. (2014) developed the XAJ-GIUH model by substituting the empirical lag-and-route runoff routing method of the original XAJ model with the GIUH routing approach. It has been demonstrated that this model produces better simulations for ungauged regions than the original XAJ model because the GIUH method can better account for the effect of geomorphologic characteristics. Recent studies have investigated the dependency of the GIUH derivation on the DEM resolution (Chavan and Srinivas, 2015; Sahoo and Jain, 2018). However, the effect of DEM resolution on the performance of the XAJ-GIUH model has not been assessed. There also remains the additional question of whether model recalibration can help minimize the dependency of the XAJ-GIUH model on the DEM resolution in order to facilitate application of the model in more regions.

Therefore, the objectives of this study were to investigate the ways in which the DEM resolution affects the derivation of GIUH and the performance of the XAJ-GIUH model and to determine whether and how model recalibration reduces the dependency of the XAJ-GIUH model on DEM resolution. The model was applied to a small catchment and a medium-sized catchment in Anhui Province, China for flood simulations. The original DEM, with a resolution of 30 m, and four resampled DEMs with resolutions of 150 m, 300 m, 450 m, and 600 m were utilized for quantitative assessment of the DEM resolution effect, as well as to determine whether better model performance can be obtained using DEMs with finer resolutions and whether the dependency of model performance on DEM resolution can be mitigated by model recalibration.

2. Study area and data

The Sankou and Xiakeng catchments, located in the southern mountainous region of Anhui Province, China, were selected as the study areas (Fig. 1). The medium-sized Sankou Catchment has a drainage area of 261 km^2, while the smaller Xiakeng Catchment has a drainage area of 89 km^2. The monsoon climate makes both humid catchments prone to floods, especially during the summer season (from May to September). Ground observations of rainfall, discharge, and pan evaporation of 42 flood events from 1968 to 2010 in the Sankou Catchment and 32 flood events from 1990 to 2006 in the Xiakeng Catchment were used to assess the performance of the XAJ-GIUH model in response to DEM resolution. According to the ground observations, the average annual precipitation of the Sankou and Xiakeng catchments were around 1 930 mm and 1 650 mm, respectively, while their annual runoff depths were 1 220 mm and 980 mm, respectively.

The original 30-m DEM data for the two catchments (Fig. 1) were provided by the Geospatial Data Cloud Site of the Computer Network Information Center at the Chinese Academy of Sciences (http://www.gscloud.cn). The 30-m DEM data were resampled to resolutions of 150 m, 300 m, 450 m, and 600 m to produce four sets of resampled DEMs. Table 1 summarizes the landscape characteristics derived from the different DEM products for the two catchments. The results showed that the drainage area generally decreased along with the DEM resolution (Table 1). However, this difference was not significant for either catchment as the grid size increased from 30 m to 600 m. Using the drainage areas derived from the 30-m DEM as a benchmark, the maximum drainage area differences

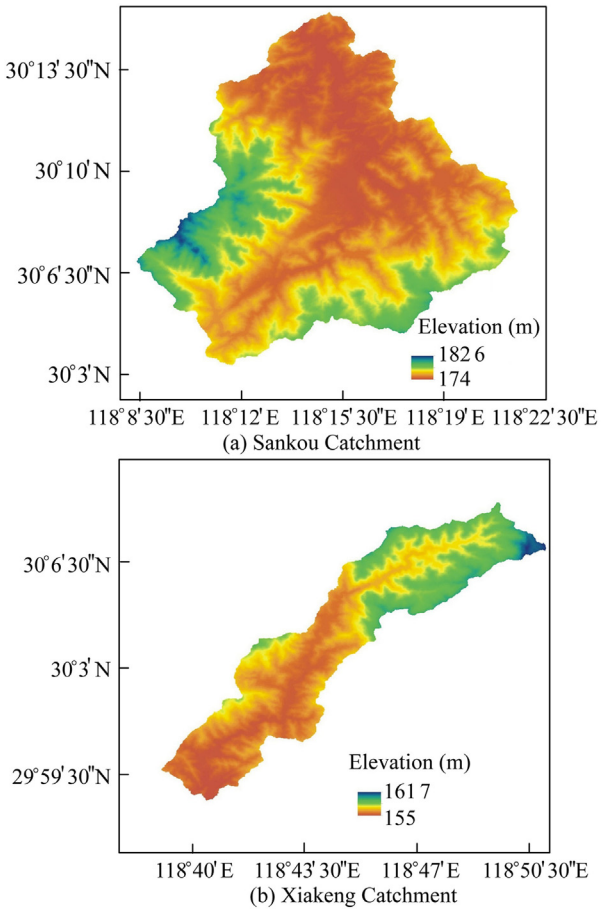


Fig. 1. Elevation maps of Sankou and Xiakeng catchments with a DEM resolution of 30 m.

were 3.4 km^2 (1.3% of the total area) for the Sankou Catchment and 1 km^2 (1.1% of the total area) for the Xiakeng Catchment. In addition, the resampled elevations, the mean slopes, and the lengths of the longest flow path decreased for both catchments as the DEM became coarser. Comparatively, the DEM resolution strongly affected the derived slopes of the study catchments (Table 1). For example, the basin-averaged slopes were reduced by 60.1% and 64.1% for the Sankou and Xiakeng catchments, respectively, when the DEM resolution increased from 30 m to 600 m (Table 1).

3. Methodology

The XAJ-GIUH model, developed on the basis of the well-tested conceptual XAJ model and the geomorphology-based GIUH approach, was employed for flood simulations in the Sankou and Xiakeng catchments. The XAJ-GIUH model was run at DEM resolutions of 30 m, 150 m, 300 m, 450 m, and 600 m, respectively, to assess the impacts of DEM resolution on flood simulations in the two study catchments.

3.1. XAJ-GIUH model

Based on the original XAJ model, the XAJ-GIUH model was developed by replacing the empirical lag-and-route runoff routing component of the original model with the GIUH routing approach, to better account for the effect of geomorphologic characteristics on runoff routing. Other physical parameterizations of hydrological processes, such as evapotranspiration, runoff generation, and runoff separation, came directly from the original XAJ model.

The basic equation for the GIUH derivation (Rodriguez-Iturbe and Valdes, 1979; Gupta et al., 1980) is

$$u(0,\ t)=f(t) \tag{1}$$

where $u(0, t)$ is the instantaneous unit hydrograph; and $f(t)$ is the probability density function of arrival time (t) of a random raindrop to the outlet. Eq. (1) is equivalent to

$$S(t)=F(t) \tag{2}$$

where $S(t)$ is the S-hydrograph; and $F(t)$ is the distribution function of arrival time.

Table 1
Topographic characteristics derived from DEMs with five different resolutions for study catchments.

Catchment	DEM resolution (m)	Drainage area (km^2)	Elevation range (m)	Mean elevation (m)	Length of longest flow path (km)	Mean slope (°)
Sankou	30	260.8	174−1 826	605.4	39.6	22.3
	150	260.7	178−1 803	605.0	37.8	17.3
	300	261.1	202−1 825	604.9	34.2	13.2
	450	259.8	225−1 777	607.7	32.1	10.5
	600	257.4	242−1 705	603.9	33.7	8.9
Xiakeng	30	88.8	155−1 617	616.8	34.8	23.7
	150	88.1	163−1 603	616.5	32.8	18.1
	300	88.4	157−1 596	609.6	31.0	13.4
	450	88.3	163−1 547	614.4	29.3	10.6
	600	87.8	190−1 543	597.2	29.3	8.5

Independent random variables l and v denote the flow path length of a raindrop, from the location it falls to the ground to the outlet, and the velocity along the flow path, respectively. The distribution function $F(t)$ can be expressed as

$$F(t)=\int_0^1 G(l)\mathrm{d}\Psi(v) \tag{3}$$

where $G(l)$ and $\Psi(v)$ are the distribution functions of l and v, respectively. Eq. (3) indicates that the flow velocity should be determined to derive the GIUH, since the flow length can be easily extracted from the DEM data. A simplification of Manning's equation (Maidment et al., 1996; Rui et al., 2008; Grimaldi et al., 2012), $V=a\sqrt{s}$, was used for the velocity estimation based on the constant coefficient (a) and land slope (s). This allows the discrete expression of Eq. (3) to be obtained:

$$F(t)=\sum_{i=1}^{m} G(ta\sqrt{s_i})[\Theta(s_i)-\Theta(s_{i-1})] \tag{4}$$

where $\Theta(s)$ is the distribution function of s, which can also be easily obtained from the DEM data; and m is the number of discrete slopes.

In this case, the Δt-period unit hydrograph derived on the basis of the GIUH concept ($u(\Delta t, t)$) is calculated as follows:

$$u(\Delta t,\ t)=F(t)-F(t-\Delta t) \tag{5}$$

where Δt is the time interval.

The XAJ-GIUH model inherits its parameters of evapotranspiration, runoff generation, and runoff separation schemes from the XAJ model. The difference is that the two parameters of the original lag-and-route method are replaced by the velocity parameter of the geomorphology-based GIUH routing method. More details on the XAJ-GIUH model and its parameters can be found in Yao et al. (2014).

3.2. Determination of model parameters

The XAJ-GIUH model was calibrated separately for the Sankou and Xiakeng catchments. About two thirds of the observed data of the two catchments were used for calibration, while the remaining data were used for validation. The shuffled complex evolution (SCE-UA) global optimization algorithm was used for model calibration (Duan et al., 1992). To address parameter equifinality, an integrated objective function (Yao et al., 2012, 2014), which consists of the relative runoff volume error (RRE), relative peak discharge error (RPE), peak time error (PTE), and Nash−Sutcliffe efficiency (NSE), was used to optimize the model parameters.

Model parameters were first calibrated at the resolution of 30 m. The calibrated parameters were directly adopted to conduct the simulations using the resampled DEMs with resolutions of 150 m, 300 m, 450 m, and 600 m to quantify the impacts of DEM resolution on model performance. Then, the model was recalibrated for the cases using the four resampled DEMs to determine whether recalibration can reduce the effect of DEM resolution on the model performance.

4. Results and discussion

4.1. Results of XAJ-GIUH model calibrated only at 30-m grid size

Table 2 lists the calibrated values of the sensitive parameters (Yao et al., 2014) of the XAJ-GIUH model using the 30-m DEM for the two study catchments. The same values of insensitive parameters were used for all cases with different DEM inputs for each catchment. These insensitive parameters are the areal mean tension water capacities of the total, upper, and lower soil layers (W_{m}, W_{um}, and W_{lm}, respectively); the evapotranspiration coefficient of the deep soil layer (C); the ratio of impervious area to the total area (I_{m}) of the basin; and the exponent of distribution of free water capacity (E_{x}). Based on the results of previous studies (Zhao and Liu, 1995; Yao et al., 2014), W_{m}, W_{um}, W_{lm}, C, I_{m}, and E_{x} were set to 120 mm, 20 mm, 60 mm, 0.18, 0.01, and 1.5, respectively. No parameter adjustment was made for the model application in the cases using the four resampled DEMs.

The GIUHs of both catchments derived from the five DEMs using the same parameter values calibrated at the 30-m grid size are illustrated in Fig. 2. When the same calibrated value of the velocity parameter (a) was used, the peak values of the GIUHs decreased for both catchments as the DEM resolution decreased from 30 m to 600 m. As described above, both flow length and slope significantly affect the derivation of GIUH. The topographic characteristics listed in Table 1 show that a coarser DEM generally resulted in a short flow length and a flat slope, mainly due to the smoothed topography from the low-resolution DEM. A short flow length tended to reduce the flow concentration time and subsequently increased the magnitude of the GIUH. A small slope had an opposite effect on the flow concentration time and the derived GIUH. Fig. 2 shows that coarser DEMs tended to attenuate the derived GIUHs. Therefore, the slope variations associated with the different DEM resolutions significantly affected the corresponding GIUHs.

The statistics of the model performance without recalibration are summarized in Table 3, including the percentages of qualified simulations; the absolute means with respect to RRE, RPE, and PTE; and the average NSE values for both calibration and validation simulations. The qualified ratios in Table 3 were calculated in accordance with the assessment standards of flood forecasting and simulation proposed by the Ministry of Water Resources of the People's Republic of China (Yao et al., 2012).

Table 2
Parameter values of XAJ-GIUH model calibrated using DEM with a resolution of 30 m in Sankou and Xiakeng catchments.

Parameter	Description	Parameter value in Sankou	Parameter value in Xiakeng
K	Ratio of potential evapotranspiration to pan evaporation	1.056	1.017
S_m	Free water capacity (mm)	38.997	58.620
K_g	Outflow coefficient of free water storage to groundwater	0.253	0.129
K_i	Outflow coefficient of free water storage to interflow	0.447	0.571
C_g	Recession constant of groundwater storage	0.965	0.951
C_i	Recession constant of interflow storage	0.407	0.102
a	Velocity parameter of the GIUH approach	1.912	2.560

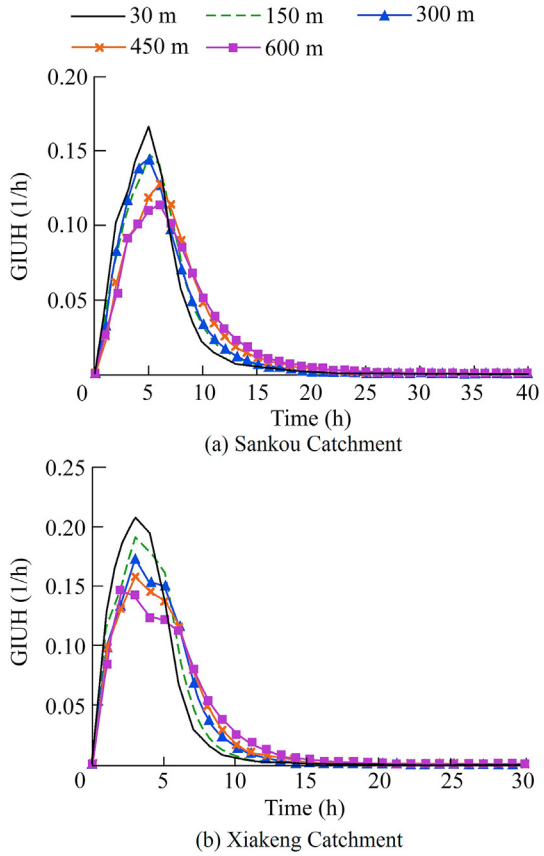


Fig. 2. Comparisons of GIUHs derived from five DEM sets for Sankou and Xiakeng catchments using parameters calibrated at a DEM resolution of 30 m.

Table 3 shows that the XAJ-GIUH simulations at different grid sizes yielded similar values of RRE and NSE but different values of RPE and PTE in the two catchments. For example, all qualified ratios with respect to RRE were 90.5% for the results with all grid sizes, and the average NSE values were almost constant for the Sankou Catchment. However, the qualified ratios of RPE decreased from 85.7% to 52.4% when the DEM resolution was reduced from 30 m to 600 m. A similar statistical pattern with respect to the DEM resolution (Table 3) was obtained for the Xiakeng Catchment. This suggested that the DEM resolution slightly affected the simulated runoff volume and the shape of the flood hydrograph. However, it strongly affected the simulated peak discharge and peak time, with a more significant impact on the former.

Fig. 3 shows the distributions of the RPE values at the five different DEM resolutions for the Sankou and Xiakeng catchments. The top, middle, and bottom of the box in Fig. 3 represent the 75th percentile, the median, and the 25th percentile, respectively, and the top, cross, and bottom lines represent the maximum, mean, and minimum values, respectively. When using the model parameters calibrated with the 30-m DEM, the RPE values worsened as the DEM resolution decreased for both catchments. For example, as the DEM resolution was changed from 30 m to 600 m in the Sankou Catchment, the minimum, median, and maximum values of RPE decreased by 8.9%, 16.7%, and 25.4%, respectively (Fig. 3). Similarly, the maximum, median, and minimum values of RPE in the Xiakeng Catchment were reduced by 8.7%, 14.7%, and 14.8%, respectively (Fig. 3).

Table 3
Accuracy statistics of XAJ-GIUH model simulations with DEMs at different resolutions using parameters calibrated with 30-m DEM.

Catchment	DEM resolution (m)	Qualified ratio			Absolute mean			Average NSE
		RRE (%)	RPE (%)	PTE (%)	RRE (%)	RPE (%)	PTE (h)	
Sankou	30	90.5	85.7	100	10.3	12.3	0.5	0.88
	150	90.5	78.6	100	10.3	12.7	0.9	0.89
	300	90.5	76.2	100	10.3	12.9	0.8	0.89
	450	90.5	71.4	97.6	10.2	15.3	1.4	0.89
	600	90.5	52.4	97.6	9.9	18.9	1.4	0.89
Xiakeng	30	84.4	84.4	93.8	10.7	11.5	1.6	0.88
	150	81.3	75.0	93.8	10.8	12.5	2.0	0.88
	300	78.1	68.8	87.5	10.8	15.1	2.2	0.88
	450	78.1	59.4	84.4	10.8	17.0	2.2	0.87
	600	81.3	50.0	75.0	10.8	20.3	2.5	0.86

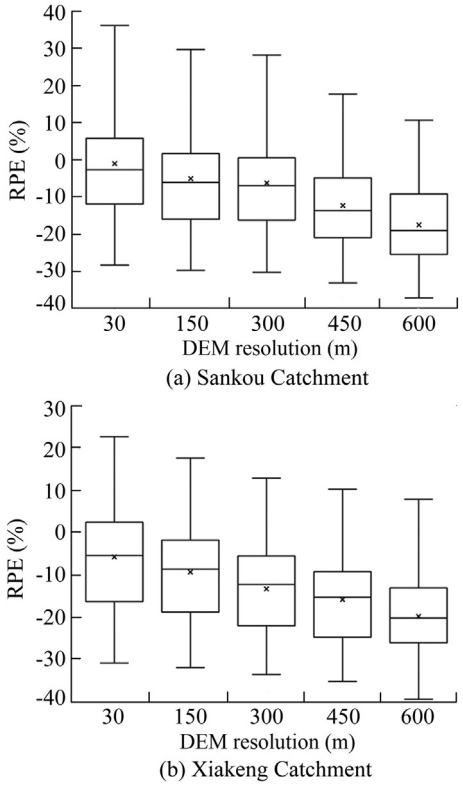


Fig. 3. Box plots of RPE statistics of XAJ-GIUH model simulations for Sankou and Xiakeng catchments using parameters calibrated with 30-m DEM.

Table 4
Parameter values of XAJ-GIUH model recalibrated using four resampled DEMs.

Catchment	DEM resolution (m)	K	S_m (mm)	K_g	K_i	C_g	C_i	a
Sankou	150	1.056	39.056	0.223	0.477	0.989	0.468	2.215
	300	1.056	40.022	0.207	0.493	0.998	0.516	2.218
	450	1.056	38.371	0.245	0.455	0.967	0.437	2.551
	600	1.056	39.728	0.210	0.490	0.989	0.448	2.670
Xiakeng	150	1.017	57.546	0.125	0.575	0.950	0.010	2.938
	300	1.017	55.652	0.108	0.592	0.980	0.013	3.275
	450	1.017	61.307	0.127	0.573	0.950	0.010	4.289
	600	1.017	59.153	0.121	0.579	0.950	0.010	4.609

4.2. Results of model recalibration for DEMs with different grid sizes

To further explore the DEM resolution effect, the XAJ-GIUH model was recalibrated at the DEM resolutions of 150 m, 300 m, 450 m, and 600 m, respectively. The recalibrated values of the sensitive model parameters for the two study catchments are listed in Table 4. The values of insensitive parameters were not adjusted for the recalibrated model. The RRE, RPE, PTE, and NSE statistics of the recalibrated model at different DEM resolutions are summarized in Table 5. In addition, Figs. 4 and 5 show the distributions of the

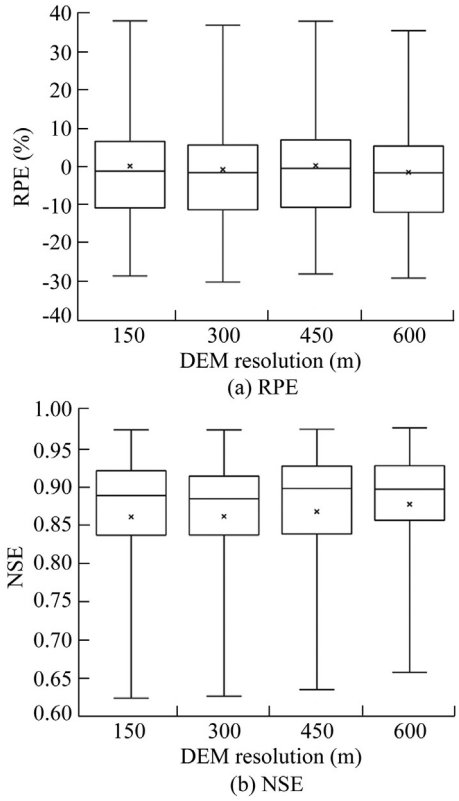


Fig. 4. Box plots of RPE and NSE statistics of model simulations using recalibrated parameters at four different DEM resolutions for Sankou Catchment.

Table 5
Accuracy statistics of XAJ-GIUH model recalibrated using resampled DEMs with different resolutions.

Catchment	DEM resolution (m)	Qualified ratio			Absolute mean			Average NSE
		RRE (%)	RPE (%)	PTE (%)	RRE (%)	RPE (%)	PTE (h)	
Sankou	150	90.5	83.3	100	10.2	12.4	0.4	0.86
	300	90.5	83.3	100	9.9	12.4	0.4	0.86
	450	90.5	83.3	100	10.3	12.3	0.4	0.87
	600	90.5	83.3	100	10.0	12.3	0.4	0.88
Xiakeng	150	84.4	84.4	93.8	10.7	11.3	1.7	0.88
	300	84.4	84.4	93.8	10.8	11.5	1.6	0.88
	450	84.4	84.4	90.6	10.7	11.1	1.7	0.86
	600	84.4	84.4	90.6	10.7	11.3	1.7	0.86

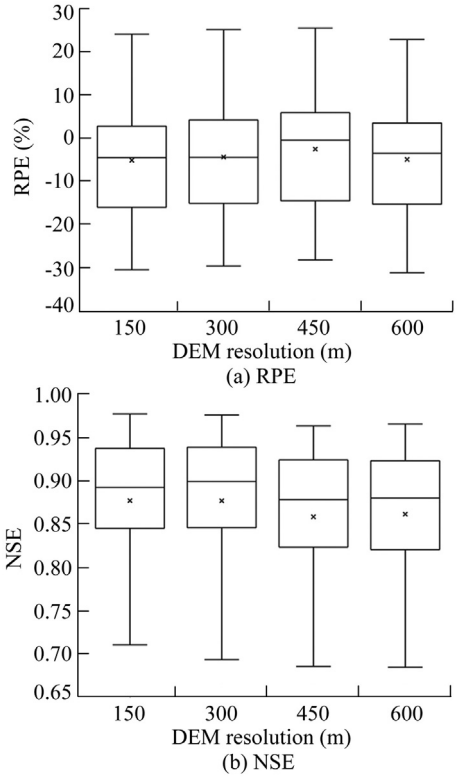


Fig. 5. Box plots of RPE and NSE statistics of model simulations using recalibrated parameters at four different DEM resolutions for Xiakeng Catchment.

RPE and NSE values of the recalibration results for the Sankou and Xiakeng catchments, respectively. The accuracy statistics of recalibration results were similar to those of the model simulations using the parameters calibrated at the DEM resolution of 30 m (Table 3 and Fig. 3). This indicated that the XAJ-GIUH model produced comparable results when the model was recalibrated at the five different DEM resolutions. The simulations using the recalibrated parameters (Table 5) showed better performances than those using the coarser DEMs and the parameters calibrated at the 30-m resolution (Table 3). However, when the model was separately calibrated at all five DEM resolutions, the results at finer DEM resolutions did not always outperform those at coarser resolutions.

4.3. Discussion

According to the statistics in Table 3 and Fig. 3, the XAJ-GIUH model yielded the best simulations for both catchments at the 30-m DEM resolution. Given that the catchment area directly affects the amount of runoff volume, a large error in the catchment area delineated from the DEM can be expected to result in a large error in the simulated runoff volume (Chaubey et al., 2005). This study showed that the impact of DEM resolution on the simulated runoff volume was relatively trivial. This may be due to the similar drainage areas extracted from DEMs with different resolutions. However, in contrast to the simulated runoff volume results, the XAJ-GIUH model produced significantly decreased peak discharges as the DEM grid size increased for both catchments. This indicated that the simulated peak discharge was strongly affected by the DEM resolution. The effect was most significant in the case with the coarsest DEM resolution (600 m), which also produced the greatest errors in the simulated peak discharge. Clearly, the DEM resolution strongly affected the derived slopes (Table 1). As a result, the GIUH derived using Eq. (4) was also influenced by the DEM resolution (Fig. 2), producing less accurate simulated peak discharges at coarse DEMs for both catchments. Additionally, the DEM resolution showed a more remarkable impact on flood simulations in the smaller Xiakeng Catchment than in the Sankou Catchment, which has a larger drainage area (Table 3 and Fig. 3).

To further demonstrate the impact of DEM resolution on the XAJ-GIUH model response without recalibration, Figs. 6 and 7 illustrate the flood simulations using the parameters calibrated at the 30-m resolution in the Sankou and Xiakeng catchments, respectively. As shown in Fig. 6, the observed peak discharge in a flood event in the Sankou Catchment was 283 m^3/s, and the simulated peak decreased from 266 m^3/s to 222 m^3/s as the DEM grid size increased from 30 m to 600 m. Likewise, a decrease in the simulated flood peak was found in the Xiakeng Catchment (Fig. 7). The simulated peak discharges decreased from 57.0 m^3/s to 45.3 m^3/s with increasing grid sizes. Figs. 6 and 7 also show that the simulated time to peak was delayed in the cases with coarser DEMs, but the

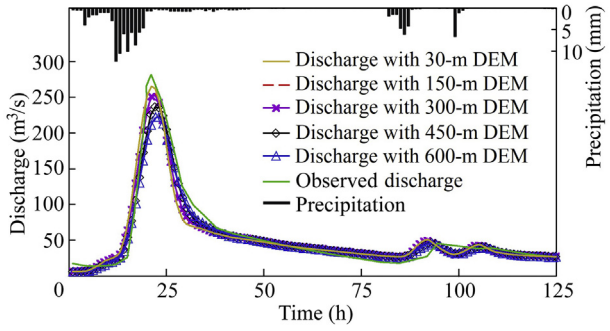


Fig. 6. Hourly hydrographs simulated by XAJ-GIUH model without recalibration for July 10, 1997 flood event in Sankou Catchment.

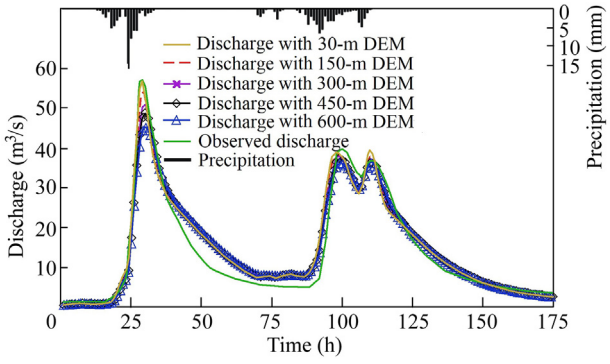


Fig. 7. Hourly hydrographs simulated by XAJ-GIUH model without recalibration for May 11, 2004 flood event in Xiakeng Catchment.

overall shapes of the simulated hydrographs were similar in these cases.

In comparison to the simulations using coarser resampled DEMs without recalibration, better simulations could be obtained when the model was recalibrated. As shown in Tables 2 and 4, the recalibrated values of the flow velocity parameter (a), which is important to the derivation of GIUHs, were significantly different when various DEM resolutions were adopted. A coarser DEM resolution tended to result in a larger a value. This confirmed the previous finding that the simulated peak discharges were underestimated by the XAJ-GIUH model simulations using the parameters calibrated at the 30-m resolution. Figs. 8 and 9 show the color-coded matrices of RPE and NSE in the Sankou and Xiakeng catchments, respectively, demonstrating model performance using the transferred parameters that were calibrated at different DEM resolutions. Clearly, the model runs with recalibrated parameters generally outperformed those using the transferred parameters. The DEM resolution had a greater effect on the flood peak than on the shape of the simulated flood hydrograph. Figs. 8 and 9 also demonstrate that the calibrated model yielded similar results at the five DEM resolutions ranging from 30 m to 600 m. The XAJ-GIUH model runs at finer DEM resolutions did not always perform better when the model was recalibrated at coarser resolutions. These results revealed that the DEM resolution impact on the model performance could be mitigated by model recalibration.

The GIUH approach is a promising runoff routing method for ungauged basins (Grimaldi et al., 2012; Hrachowitz et al., 2013) because it can make the best use of widely available DEM data. However, this study indicated that the DEM resolution significantly affects the derived GIUHs and GIUH-based flood simulations. In addition, given that the runoff velocity is difficult to determine directly, the velocity parameter should be estimated to derive GIUHs. Accordingly, regionalization of the velocity parameter is usually necessary for application of the GIUH approach to ungauged regions (Yao et al., 2014; Chen et al., 2019). Based on the XAJ-GIUH model simulation results, the effect of DEM resolution should be considered in regionalization of the velocity parameter. We suggest that the velocity parameter be calibrated at the same DEM resolution for regionalization. Otherwise, recalibration is necessary when the DEM resolution changes. The other solution is to develop a quantitative relationship between the

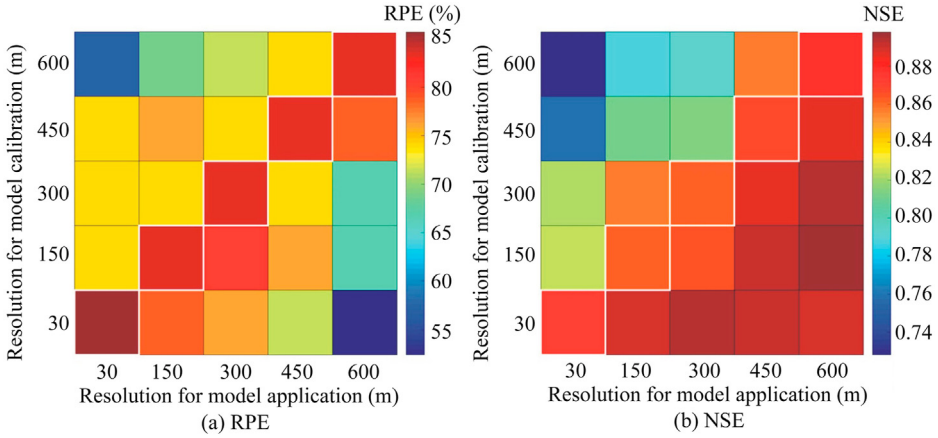


Fig. 8. Color-coded matrices of RPE and NSE in XAJ-GIUH model simulations using transferred parameter values that were calibrated at different DEM resolutions in Sankou Catchment.

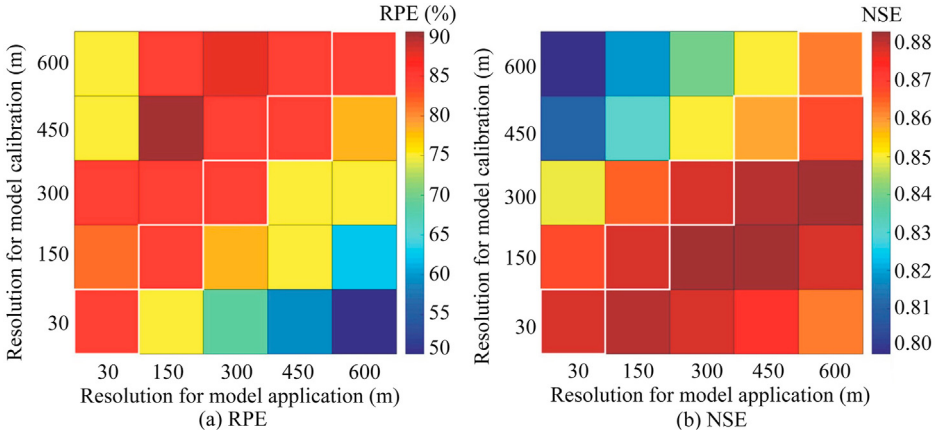


Fig. 9. Color-coded matrices of RPE and NSE in XAJ-GIUH model simulations using transferred parameter values that were calibrated at different DEM resolutions in Xiakeng Catchment.

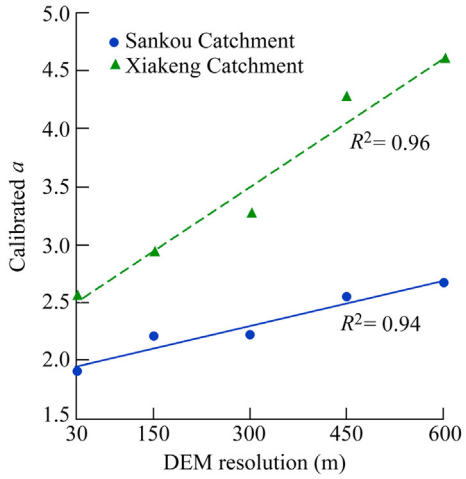


Fig. 10. Relationships between calibrated velocity parameter (a) and DEM resolution in Sankou and Xiakeng catchments.

parameter a and the DEM resolution. As an example, Fig. 10 illustrates the relationship between the calibrated a value and the corresponding DEM resolution in the Sankou and Xiakeng catchments, showing that a had a clear linear relationship with the DEM resolution in both catchments. This indicates that model recalibration might be skipped if a general relationship between the velocity parameter and the DEM resolution can be derived. In addition, Fig. 10 shows that the trendline slope for the Xiakeng Catchment was larger than that for the Sankou Catchment, demonstrating that the DEM resolution had a relatively larger impact on the XAJ-GIUH model performance in a smaller catchment than in a larger catchment.

5. Conclusions

This study assessed the effect of DEM resolution on the XAI-GIUH model-based flood simulations in a small catchment and a medium-sized catchment. DEMs with five different resolutions (30 m, 150 m, 300 m, 450 m, and 600 m) were utilized for the quantitative evaluation. Coarser DEMs (with larger grid sizes) were obtained by resampling the original 30-m DEM. The parameters of the XAJ-GIUH model were calibrated at the original 30-m DEM resolution and then directly transferred to the four model runs using coarser DEMs. Afterwards, the model was recalibrated at the resolutions of 150 m, 300 m, 450 m, and 600 m to further evaluate the DEM resolution effect. The main conclusions can be summarized as follows:

(1) The topographic attributes extracted from the five DEM data sets showed that the drainage areas of the two study catchments were only slightly affected by DEM resolution. In contrast, DEM resolution significantly influenced the flow length and slope, which are important to the derivation of GIUH.

(2) The simulated GIUH peak discharges tended to decrease in both catchments as the DEM resolution became coarser. This explains why the model runs using coarser DEMs without recalibration consistently underestimated the peak discharges. Thus, the effect of DEM resolution on the XAJ-GIUH model performance in small and medium-sized catchments should be considered. This effect was more pronounced in the smaller catchment (i.e., the Xiakeng Catchment).

(3) Model recalibration showed that the values of the velocity parameter (a) used for derivation of GIUHs always increased in both catchments as the DEM resolution became coarser. This finding confirmed the conclusion that relatively poorer peak simulations were obtained without recalibration. The effect of DEM resolution on the performance of the XAJ-GIUH model can be mitigated by model recalibration.

Declaration of competing interest

The authors declare no conflicts of interest.

Acknowledgements

The authors acknowledge the Hydrology Bureau of Anhui Province, China for kindly providing the hydrological data.

References

Beven, K., 2012. Rainfall-Runoff Modelling: The Primer, Second Ed. Wiley-Blackwell, Chichester.

Beven, K., 2019. How to make advances in hydrological modelling. Hydrol. Res. 50(6), 1481−1494. https://doi.org/10.2166/nh.2019.134.

Bhadra, A., Panigrahy, N., Singh, R., Raghuwanshi, N.S., Mal, B.C., Tripathi, M.P., 2008. Development of a geomorphological instantaneous unit hydrograph model for scantily gauged watersheds. Environ. Model. Softw. 23(8), 1013−1025. https://doi.org/10.1016/j.envsoft.2007.08.008.

Blair, G.S., Beven, K., Lamb, R., Bassett, R., Cauwenberghs, K., Hankin, B., Dean, G., Hunter, N., Edwards, L., Nundloll, V., Samreen, F., Simm, W., Towe, R., 2019. Models of everywhere revisited: A technological perspective. Environ. Model. Softw. 122, 104521. https://doi.org/10.1016/j.envsoft.2019.104521.

Chao, L.J., Zhang, K., Li, Z.J., Wang, J.F., Yao, C., Li, Q.L., 2019. Applicability assessment of the CASCade Two Dimensional SEDiment (CASC2D-SED) distributed hydrological model for flood forecasting across four typical medium and small watersheds in China. J. Flood Risk Manag. 12, e12518. https://doi.org/10.1111/jfr3.12518.

Chao, L.J., Zhang, K., Yang, Z.L., Wang, J., Liu, P., Liang, J., Li, Z.J., Gu, Z., 2021. Improving flood simulation capability of the WRF-hydro-RAPID model using a multi-source precipitation merging method. J. Hydrol. 592, 125814. https://doi.org/10.1016/j.jhydrol.2020.125814.

Chaubey, I., Cotter, A.S., Costello, T.A., Soerens, T.S., 2005. Effect of DEM data resolution on SWAT output uncertainty. Hydrol. Process. 19(3), 621−628. https://doi.org/10.1002/hyp.5607.

Chavan, S.R., Srinivas, V.V., 2015. Effect of DEM source on equivalent Horton−Strahler ratio based GIUH for catchments in two Indian river basins. J. Hydrol. 528, 463−489. https://doi.org/10.1016/j.jhydrol.2015.06.049.

Chen, Y.B., Shi, P., Ji, X.M., Qu, S.M., Zhao, L.L., Dong, F.C., 2019. New method to calculate the dynamic factor-flow velocity in geomorphologic instantaneous unit hydrograph. Sci. Rep. 9, 14201. https://doi.org/10.1038/S41598-019-50723-X.

Clark, M.P., Bierkens, M.F.P., Samaniego, L., Woods, R.A., Uijlenhoet, R., Bennett, K.E., Pauwels, V.R.N., Cai, X., Wood, A.W., Peters-Lidard, C.D., 2017. The evolution of process-based hydrologic models: Historical challenges and the collective quest for physical realism. Hydrol. Earth Syst. Sci. 21(7), 3427−3440. https://doi.org/10.5194/hess-21-3427-2017.

DaRos, D., Borga, M., 1997. Use of digital elevation model data for the derivation of the geomorphological instantaneous unit hydrograph. Hydrol.

Process. 11(1), 13−33. https://doi.org/10.1002/(SICI)1099-1085(199701)11:1<13::AID-HYP400>3.0.CO;2-M.

Dixon, B., Earls, J., 2009. Resample or not?! Effects of resolution of DEMs in watershed modeling. Hydrol. Process. 23(12), 1714−1724. https://doi.org/10.1002/hyp.7306.

Duan, Q., Sorooshian, S., Gupta, V., 1992. Effective and efficient global optimization for conceptual rainfall-runoff models. Water Resour. Res. 28(4), 1015−1031. https://doi.org/10.1029/91WR02985.

Gong, J.F., Yao, C., Li, Z.J., Chen, Y.F., Huang, Y.C., Tong, B.X., 2021. Improving the food forecasting capability of the Xinanjiang model for small- and medium-sized ungauged catchments in South China. Nat. Hazards 106, 2077−2109. https://doi.org/10.1007/s11069-021-04531-0.

Grimaldi, S., Petroselli, A., Nardi, F., 2012. A parsimonious geomorphological unit hydrograph for rainfall-runoff modelling in small ungauged basins. Hydrol. Sci. J. 57(1), 73−83. https://doi.org/10.1080/02626667.2011.636045.

Gupta, V., Waymire, E., Wang, C., 1980. A representation of an instantaneous unit hydrograph from geomorphology. Water Resour. Res. 16(5), 855−862. https://doi.org/10.1029/WR016i005p00855.

Habtezion, N., Tahmasebi Nasab, M., Chu, X., 2016. How does DEM resolution affect microtopographic characteristics, hydrologic connectivity, and modelling of hydrologic processes? Hydrol. Process. 30(25), 4870−4892. https://doi.org/10.1002/hyp.10967.

Hrachowitz, M., Savenije, H.H.G., Blöschl, G., McDonnell, J.J., Sivapalan, M., Pomeroy, J.W., Arheimer, B., Blume, T., Clark, M.P., Ehret, U., et al., 2013. A decade of predictions in ungauged basins (PUB): A review. Hydrol. Sci. J. 58(6), 1198−1255. https://doi.org/10.1080/02626667.2013.803183.

Khaing, Z.M., Zhang, K., Sawano, H., Shrestha, B.B., Sayama, T., Nakamura, K., 2019. Flood hazard mapping and assessment in data-scarce Nyaungdon area, Myanmar. PLoS One 14(11), e0224558. https://doi.org/10.1371/journal.pone.0224558.

López-Vicente, M., Álvarez, S., 2018. Influence of DEM resolution on modelling hydrological connectivity in a complex agricultural catchment with woody crops. Earth Surf. Process. Landf. 43(7), 1403−1415. https://doi.org/10.1002/esp.4321.

Maidment, D., Olivera, F., Calver, A., Eatherall, A., Fraczek, W., 1996. Unit hydrograph derived from a spatially distributed velocity field. Hydrol. Process. 10, 831−844. https://doi.org/10.1002/(SICI)1099-1085(199606)10:6<831::AID-HYP374>3.0.CO;2-N.

Moglen, G.E., Hartman, G.L., 2001. Resolution effects on hydrologic modeling parameters and peak discharge. J. Hydrol. Eng. 6(6), 490−497. https://doi.org/10.1061/(Asce)1084-0699(2001)6:6(490).

Mu, D.R., Luo, P.P., Lyu, J., Zhou, M.M., Huo, A.D., Duan, W.L., Nover, D., He, B., Zhao, X.L., 2021. Impact of temporal rainfall patterns on flash floods in Hue City, Vietnam. J. Flood Risk Manag. 14(1), e12668. https://doi.org/10.1111/jfr3.12668.

Munoth, P., Goyal, R., 2019. Effects of DEM source, spatial resolution and drainage area threshold values on hydrological modeling. Water Resour. Manag. 33(6), 3303−3319. https://doi.org/10.1007/s11269-019-02303-x.

Reddy, A.S., Reddy, M.J., 2015. Evaluating the influence of spatial resolutions of DEM on watershed runoff and sediment yield using SWAT. J. Earth Syst. Sci. 124(7), 1517−1529. https://doi.org/10.1007/s12040-015-0617-2.

Rodriguez-Iturbe, I., Valdes, J., 1979. The geomorphological structure of hydrologic response. Water Resour. Res. 15(6), 1409−1420. https://doi.org/10.1029/WR015i006p01409.

Rui, X.F., Yu, M., Liu, F.G., Gong, X.L., 2008. Calculation of watershed flow concentration based on the grid drop concept. Water Sci. Eng. 1(1), 1−9. https://doi.org/10.1016/S1674-2370(15)30013-2.

Sahoo, R., Jain, V., 2018. Sensitivity of drainage morphometry based hydrological response (GIUH) of a river basin to the spatial resolution of DEM data. Comput. Geosci. 111, 78−86. https://doi.org/10.1016/j.cageo.2017.10.001.

Valeo, C., Moin, S.M.A., 2000. Grid-resolution effects on a model for integrating urban and rural areas. Hydrol. Process. 14(14), 2505−2525. https://doi.org/10.1002/1099-1085(20001015)14:14<2505::AID-HYP111>3.0.CO;2-3.

Vieux, B.E., 2001. Distributed Hydrologic Modeling Using GIS. Kluwer Academic Publishers, Dordrecht.

Vivoni, E.R., Ivanov, V.Y., Bras, R.L., Entekhabi, D., 2005. On the effects of triangulated terrain resolution on distributed hydrologic model response. Hydrol. Process. 19(11), 2101−2122. https://doi.org/10.1002/hyp.5671.

Wei, X.D., Wang, N., Luo, P.P., Yang, J., Zhang, J., Lin, K.L., 2021. Spatio-temporal assessment of land marketization and its driving forces for sustainable urban-rural development in Shaanxi Province in China. Sustainability 13(14), 7755. https://doi.org/10.3390/su13147755.

Wilby, R.L., 2019. A global hydrology research agenda fit for the 2030s. Hydrol. Res. 50(6), 1464−1480. https://doi.org/10.2166/nh.2019.100.

Xu, C., 2021. Issues influencing accuracy of hydrological modeling in a changing environment. Water Sci. Eng. 14(2), 167−170. https://doi.org/10.1016/j.wse.2021.06.005.

Yang, P., Ames, D.P., Fonseca, A., Anderson, D., Shrestha, R., Glenn, N.F., Cao, Y., 2014. What is the effect of LiDAR-derived DEM resolution on large-scale watershed model results? Environ. Model. Softw. 58, 48−57. https://doi.org/10.1016/j.envsoft.2014.04.005.

Yao, C., Li, Z.J., Bao, H.J., Yu, Z.B., 2009. Application of a developed grid-Xinanjiang model to Chinese watersheds for flood forecasting purpose. J. Hydrol. Eng. 14(9), 923−934. https://doi.org/10.1061/(Asce)He.1943-5584.0000067.

Yao, C., Li, Z.J., Yu, Z.B., Zhang, K., 2012. A priori parameter estimates for a distributed, grid-based Xinanjiang model using geographically based information. J. Hydrol. 468−469, 47−62. https://doi.org/10.1016/j.jhydrol.2012.08.025.

Yao, C., Zhang, K., Yu, Z.B., Li, Z.J., Li, Q.L., 2014. Improving the flood prediction capability of the Xinanjiang model in ungauged nested catchments by coupling it with the geomorphologic instantaneous unit hydrograph. J. Hydrol. 517, 1035−1048. https://doi.org/10.1016/j.jhydrol.2014.06.037.

Yao, C., Ye, J.Y., He, Z.X., Bastola, S., Zhang, K., Li, Z.J., 2019. Evaluation of flood prediction capability of the distributed grid-Xinanjiang model driven by weather research and forecasting precipitation. J. Flood Risk Manag. 12, e12544. https://doi.org/10.1111/jfr3.12544.

Zha, X.B., Luo, P.P., Zhu, W., Wang, S.T., Lyu, J.Q., Zhou, M.M., Huo, A.D., Wang, Z.H., 2021. A bibliometric analysis of the research on sponge city: Current situation and future development direction. Ecohydrology 14(7), e2328. https://doi.org/10.1002/eco.2328.

Zhang, K., Xue, X.W., Hong, Y., Gourley, J.J., Lu, N., Wan, Z.M., Hong, Z., Wooten, R., 2016. iCRESTRIGRS: A coupled modeling system for cascading flood−landslide disaster forecasting. Hydrol. Earth Syst. Sci. 20(12), 5035−5048. https://doi.org/10.5194/hess-20-5035-2016.

Zhang, K., Niu, J., Li, X., Chao, L., 2021. Comparison of artificial intelligence flood forecasting models in China's semi-arid and semi-humid regions. Water Resour. Prot. 37(1), 28−35. https://doi.org/10.3880/j.issn.1004-6933.2021.01.005 (in Chinese).

Zhao, R., 1992. The Xinanjiang model applied in China. J. Hydrol. 135, 371−381. https://doi.org/10.1016/0022-1694(92)90096-E.

Zhao, R., Liu, X., 1995. The Xinanjiang model. In: Singh, V. (Ed.), Computer Models of Watershed Hydrology. Water Resources Publications, Littleton, pp. 215−232.

Zheng, X., Tarboton, D.G., Maidment, D.R., Liu, Y.Y., Passalacqua, P., 2018. River channel geometry and rating curve estimation using height above the nearest drainage. J. Am. Water Resour. Assoc. 54(4), 785−806. https://doi.org/10.1111/1752-1688.12661.

Zhu, Y.H., Luo, P.P., Zhang, S., Sun, B., 2020. Spatiotemporal analysis of hydrological variations and their impacts on vegetation in semiarid areas from multiple satellite data. Rem. Sens. 12(24), 4177. https://doi.org/10.3390/Rs12244177.